



HAL
open science

Synthesis of molybdates $Zn_{1-x}Co_xMoO_4$ ($0 \leq x \leq 1$), by decomposition of the precursors developed by the glycine-nitrate process (GNP), and their characterization

Hind Lakhlifi, Youssef El Jabbar, Rachida El Ouatib, Lahcen Er-Rakho,
Bernard Durand, Sophie Guillemet

► To cite this version:

Hind Lakhlifi, Youssef El Jabbar, Rachida El Ouatib, Lahcen Er-Rakho, Bernard Durand, et al.. Synthesis of molybdates $Zn_{1-x}Co_xMoO_4$ ($0 \leq x \leq 1$), by decomposition of the precursors developed by the glycine-nitrate process (GNP), and their characterization. *Materials Science in Semiconductor Processing*, 2020, 114, pp.105054. 10.1016/j.mssp.2020.105054 . hal-03851478v1

HAL Id: hal-03851478

<https://hal.science/hal-03851478v1>

Submitted on 1 Dec 2020 (v1), last revised 23 Nov 2022 (v2)

HAL is a multi-disciplinary open access archive for the deposit and dissemination of scientific research documents, whether they are published or not. The documents may come from teaching and research institutions in France or abroad, or from public or private research centers.

L'archive ouverte pluridisciplinaire **HAL**, est destinée au dépôt et à la diffusion de documents scientifiques de niveau recherche, publiés ou non, émanant des établissements d'enseignement et de recherche français ou étrangers, des laboratoires publics ou privés.



Open Archive Toulouse Archive Ouverte

OATAO is an open access repository that collects the work of Toulouse researchers and makes it freely available over the web where possible

This is an author's version published in:
<http://oatao.univ-toulouse.fr/26801>

Official URL

DOI : <https://doi.org/10.1016/j.mssp.2020.105054>

To cite this version: Lakhlifi, Hind and El Jabbar, Youssef and El Ouatib, Rachida and Er-Rakho, Lahcen and Durand, Bernard and Guillemet-Fritsch, Sophie *Synthesis of molybdates $Zn_{1-x}Co_xMoO_4$ ($0 \leq x \leq 1$), by decomposition of the precursors developed by the glycine-nitrate process (GNP), and their characterization.* (2020) *Materials Science in Semiconductor Processing*, 114. 105054. ISSN 1369-8001

Any correspondence concerning this service should be sent to the repository administrator: tech-oatao@listes-diff.inp-toulouse.fr

Synthesis of molybdates $Zn_{1-x}Co_xMoO_4$ ($0 \leq x \leq 1$), by decomposition of the precursors developed by the glycine-nitrate process (GNP), and their characterization

Hind Lakhliif^{a,*}, Youssef El Jabbar^a, Rachida El Ouatib^a, Lahcen Er-Rakho^a, Bernard Durand^b, Sophie Guillemet-Fritsch^b

^a Laboratoire de Physico-chimie des Matériaux Inorganiques, Faculté des Sciences Aïn Chock, Université Hassan II, Bp. 5366 Mâarif, Casablanca, Morocco

^b Institut Carnot CIRIMAT, CNRS Université de Toulouse, 118 Route de Narbonne, 31062, Toulouse Cedex 9, France

ABSTRACT

Keywords:
Molybdates
XRD
Synthesis
Morphology
Glycine-nitrate process
Solid state

Nanocrystals of zinc-cobalt molybdate ($Zn_{1-x}Co_xMoO_4$) were prepared by the glycine-nitrate process (GNP) route with a glycine/nitrate ratio of 2:3 and compared to the solid state synthesis. The obtained powders were characterized by thermal analysis (TGA-TDA), X-ray powder diffraction (XRD), Fourier transform infrared spectroscopy (FTIR) and Raman spectroscopy. The morphology was examined by scanning electron microscopy (SEM) and Brunauer–Emmett–Teller (BET). The particle size was determined by transmission electron microscopies (TEM). UV-Visible spectroscopy and CIE L*a*b* colorimetric parameters have been used for the colour characterisation and measurement. The compounds obtained present two single-phased domains regardless of the synthesis method. The first domain of blue colour corresponding to a level of cobalt x such as: $0 = x \leq 0.3$, isostructural with α - $ZnMoO_4$ of triclinic symmetry and the second domain of green colour, for cobalt x levels such as: $0.45 = x \leq 1$ isostructural with α - $CoMoO_4$ of monoclinic structure. The $Zn_{0.7}Co_{0.3}MoO_4$ powders obtained at 700 °C by GNP route and synthesized in acidic environment were formed of particles of quasi-spherical morphology, with average size of crystallites estimated between 80 - 140 nm.

1. Introduction

The molybdates of bivalent elements known by the formula $AMoO_4$ (A = bivalent element) have been widely studied in recent years because of their remarkable optical properties [1,2]. These oxides are thermochromic and piezochromic materials that present phase transitions associated with strong changes in colour and the doping by various chemical elements can be modify temperatures and pressure transitions [3]. Metal molybdates with monoclinic/triclinic systems have various potential uses, such as for photoluminescence, semiconductor lasers, magnetism, lithium-ion batteries, microwave applications, catalysis, photoelectric devices, photonic crystals, and chemical reactors [4–7].

The present paper focuses on the synthesis of zinc molybdate substituted with cobalt. In this structure, the zinc atoms are bound to six oxygen atoms, forming distorted octahedral clusters $[ZnO_6]$ [8]. Molybdenum atoms are associated with four oxygen atoms, resulting in tetrahedral clusters $[MoO_4]$, while the Zn^{2+} ions occupy two sites of different symmetry: octahedral and bipyramidal triangular bases [9].

The presence of the cobalt ions in these sites induces differentiable colours resulting from the d-d electron transitions [10]. Several synthesis methods have been used to synthesize the molybdate $AMoO_4$, such as the solvothermal method [11], co-precipitation [12,13], the Pechini method [14], the molten salt method [15], and the sol-gel route [16]. This work presents a synthesis of cobalt-zinc molybdate using the Glycine-Nitrate-Process (GNP) route based on exothermic redox reactions. Compared to the conventional solid state method, this method creates more reactive precursors that lead to powders with a high specific surface area at low annealing temperatures.

2. Methods and materials

The reagents used to develop the precursors of the molybdate $Zn_{1-x}Co_xMoO_4$ are zinc nitrate ($Zn(NO_3)_2 \cdot 6H_2O$) (Aldrich, 98%), cobalt nitrate ($Co(NO_3)_2 \cdot 6H_2O$) (Aldrich, 98%), and ammonium heptamolybdate ($(NH_4)_6Mo_7O_{24} \cdot 4H_2O$) (Acros, 99%). These reagents were mixed in stoichiometric proportions. Glycine was then introduced in a

* Corresponding author.

E-mail address: lakhliifhind21@gmail.com (H. Lakhliif).

molar ratio of glycine/nitrates of 2:3. After evaporation at 110 °C, the precursors obtained were pre-calcined at 300 °C for 12 h. The resulting black powder was heat treated for 2 h at a determined temperature. Depending on the amount of cobalt ($0 = x \leq 1$), different colours were obtained after grinding. The synthesized powders were characterized using an x-ray diffractometer (Bruker D8 Advance equipped with a detector LynxEye, $\text{CuK}\alpha$, $\lambda = 1.5406 \text{ \AA}$), and the infrared spectra were taken using an FTIR spectrometer (IR Affinity-1S Shimadzu). The Raman spectra were recorded with a LabRAM HR 800 (Horiba Jobin-Yvon) spectrometer, and UV-vis measurements were taken with a Perkin Elmer Lambda 35 spectrophotometer. The morphology of the powders was examined using scanning electronic microscopy (JEOL JSM 6400), and the measurements of specific surface areas were determined using the BET method (Micrometrics Flowsorb II 2300). The colour parameters (L^* , a^* , b^*) were measured using the CIE Lab system colorimeter (CR-400/410, KONICA MINOLTA).

3. Results and discussion

3.1. Thermal decomposition

Thermal analysis (TGA/DTA) was performed to monitor the thermal decomposition process of the precursors synthesized by GNP route, and to estimate the calcination temperature (Fig. 1(a) and (b)). Fig. 1(a) presents the thermal decomposition of the precursor of $\text{Zn}_{0.7}\text{Co}_{0.3}\text{MoO}_4$ which occurred over several steps. An initial weight loss of 9% was observed between 50 °C and 150 °C, corresponding to the elimination of superficially adsorbed water. Pyrolysis showed a weight loss of 5% in the temperature range of 200–310 °C and a more significant loss of 12% at 450 °C, which was accompanied by an exothermic peak at 450 °C, and a more significant loss of 12% at 450 °C, which was accompanied by an exothermic peak. For the precursor of the molybdates $\text{Zn}_{0.4}\text{Co}_{0.6}\text{MoO}_4$ (Fig. 1(b)), the loss attributed

to the elimination of water was less (3%), and the combustion of organic water occurred in one step, involving a weight loss of 8% accompanied by an exothermic peak at 430 °C. Beyond 600 °C, no weight loss was observed, indicating that the decomposition was complete and confirming that 700 °C was the most appropriate temperature for obtaining pure phases free of organic residue.

Fig. 2(a) and (b) show the thermogravimetric analysis in air of the mixtures of nitrates used for the preparation by the solid-state reactions of the molybdates $\text{Zn}_{0.8}\text{Co}_{0.2}\text{MoO}_4$ and $\text{Zn}_{0.4}\text{Co}_{0.6}\text{MoO}_4$ powders. The observed weight losses were 20% and 36%, respectively. These losses agreed with those calculated for dehydration and the decomposition of nitrates (19% for the compound with $x = 0.2$ and 33% for $x = 0.6$). These transformations are shown by endothermic peaks on the DTA curves. No phenomena were observed above 500 °C; thus, decomposition was complete.

3.2. X-ray diffraction characterisation

Fig. 3 shows the XRD patterns of powders prepared using the GNP route in an acidic medium ($\text{pH} = 3$), treated at 700 °C for 2 h, and ground. As shown in Fig. 4, the following observations were made:

- For $0 = x \leq 0.30$, the powder was monophased and isostructural with triclinic $\alpha\text{-ZnMoO}_4$ (JCPDS file No. 070-5365).
- For $x = 0.35$ and $x = 0.40$, the powder presents two-phase mixture, one majority isostructural phase with monoclinic $\alpha\text{-CoMoO}_4$ (JCPDS file No. 073-1331) and minority phase isostructural with triclinic $\alpha\text{-ZnMoO}_4$ (JCPDS file: No. 070-5365).
- For $0.45 = x \leq 1$, the powder was monophased and isostructural with $\alpha\text{-CoMoO}_4$.

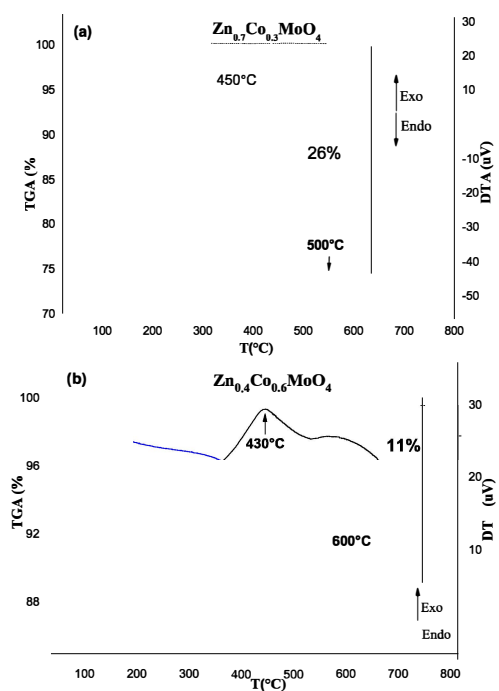


Fig. 1. TGA DTA curves of (a) the $\text{Zn}_{0.7}\text{Co}_{0.3}\text{MoO}_4$ and (b) the $\text{Zn}_{0.4}\text{Co}_{0.6}\text{MoO}_4$ precursors prepared by GNP route.

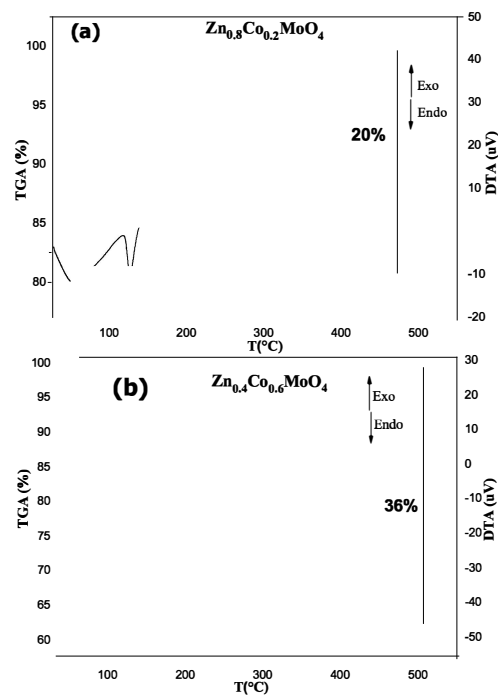


Fig. 2. TGA DTA curves of (a) the $\text{Zn}_{0.8}\text{Co}_{0.2}\text{MoO}_4$ and (b) the $\text{Zn}_{0.4}\text{Co}_{0.6}\text{MoO}_4$ precursors prepared by solid-state reactions.

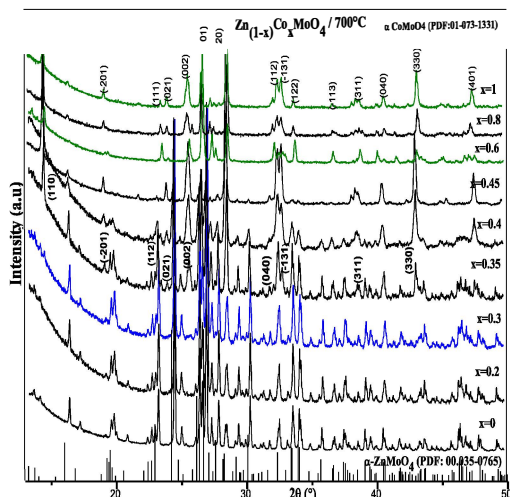


Fig. 7. XRD patterns of $Zn_{1-x}Co_xMoO_4$ ($0 \leq x \leq 1$) compounds prepared at $700^\circ C$ by solid state reactions.

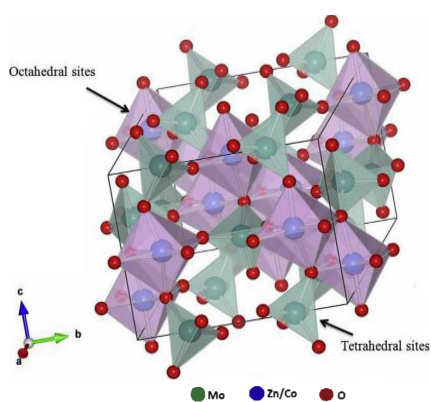


Fig. 8. Ball and stick representation of crystal structure of the $Zn_{1-x}Co_xMoO_4$.

3.5. Microstructural characterization

The SEM images for $Zn_{0.7}Co_{0.3}MoO_4$ prepared by GNP route show a powder formed of agglomerated particles of varying morphology (Fig. 11 (a)) and for the $Zn_{0.4}Co_{0.6}MoO_4$ (Fig. 11 (b)) an advanced pre-sintering state which can be attributed to the high cobalt rate. While the powders prepared by solid state reactions consisted by agglomerates of grains as revealed in Fig. 12(a) and (b). The TEM micrograph for $Zn_{0.7}Co_{0.3}MoO_4$ powder prepared by GNP route (Fig. 13 (a)) reveal elementary grains of more or less spherical shape with average size estimated between 80 and 140 nm. While that prepared by solid state reaction (Fig. 13 (b)) show agglomerated particles with average size of a few micrometers.

3.6. Colours analysis

The colour parameters (L^* , a^* , b^*) of the powders obtained by GNP

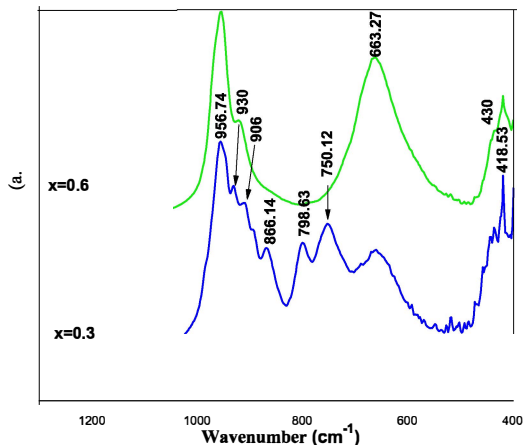


Fig. 9. FT-IR spectra of $Zn_{1-x}Co_xMoO_4$ ($x = 0.3$ and $x = 0.6$) powders obtained at $700^\circ C$.

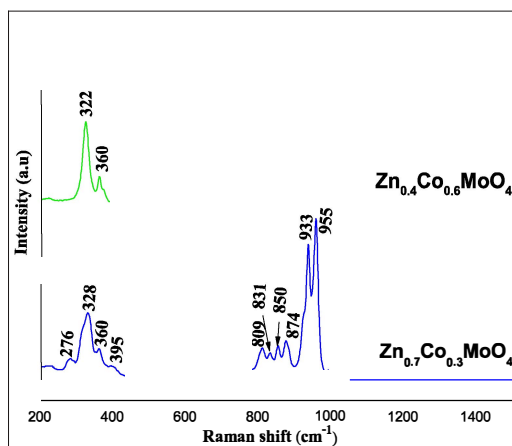


Fig. 10. Raman Spectra of the molybdates $Zn_{0.7}Co_{0.3}MoO_4$ and $Zn_{0.4}Co_{0.6}MoO_4$ prepared by the GNP route.

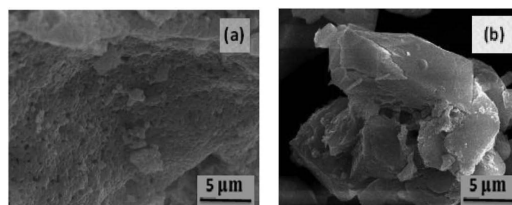


Fig. 11. SEM micrographs of the compositions $x = 0.3$ (a) and $x = 0.6$ (b) prepared by GNP route.

method and by solid state reactions were measured in the CIE Lab system using a CR-400/410 colorimeter. The evolution of these parameters as a function of the x composition and the pH was given in Fig. 14 (a)-(b) and Fig. 15 (a)-(b) for the compounds obtained by the GNP route and

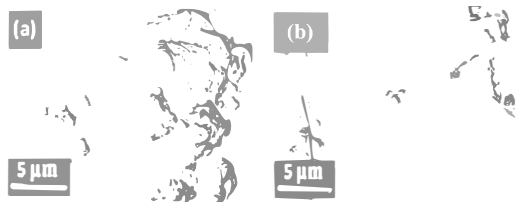


Fig. 12. SEM micrographs of the compositions $x = 0.3$ (a) and $x = 0.6$ (b) prepared by solid state reactions.

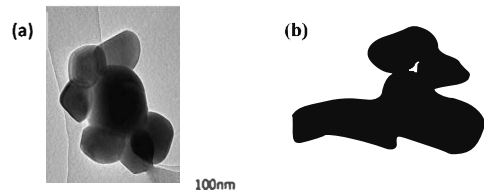


Fig. 13. TEM micrographs of $Zn_{0.7}Co_{0.3}MoO_4$ prepared by (a) GNP route and (b) solid state reactions.

those obtained by solid state reactions, respectively. The component ($-b^*$) characterizing the blue colour, has a maximum for compositions $0.2 \leq x \leq 0.3$ regardless of the method of synthesis adopted. In the case of samples synthesized by GNP route, the evolution of colour parameters

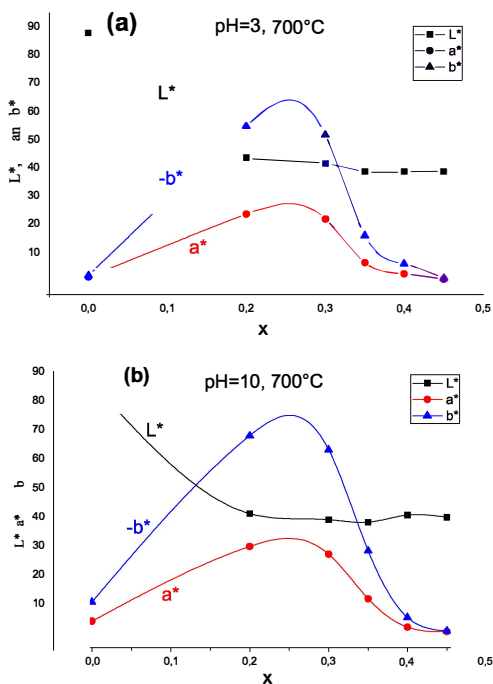


Fig. 14. Evolution of the colour parameters of $Zn_{1-x}Co_xMoO_4$ powders with $0 \leq x \leq 0.45$ obtained by GNP route at pH = 3 (a) and pH = 10 (b).

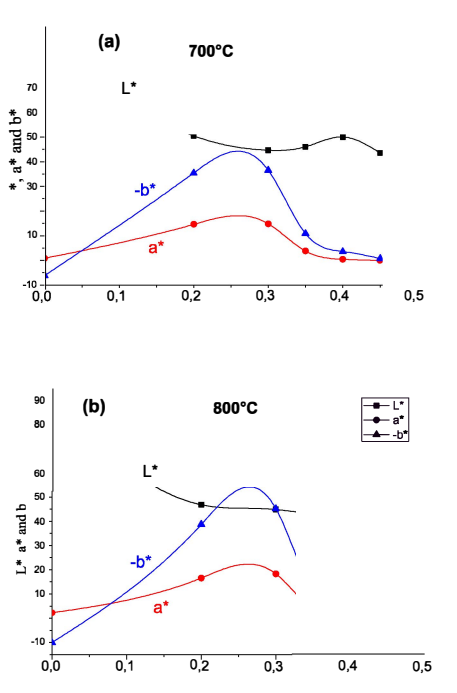


Fig. 15. Evolution of the colour parameters of $Zn_{1-x}Co_xMoO_4$ powders with $0 \leq x \leq 0.45$ obtained by solid state reactions at (a) 700 °C and (b) 800 °C.

shows that the blue colour appears to develop more for the composition $x = 0.25$ in the basic medium. It seems that the degree of blueness for the samples prepared by solid state increase with annealing temperature.

The origin of the colour difference between $Zn_{0.7}Co_{0.3}MoO_4$ compound noted ϕ_T and $Zn_{0.4}Co_{0.6}MoO_4$ compound noted ϕ_M was studied UV-visible spectroscopy (Fig. 16). Whatever the used synthesis method, the spectrum of the triclinical molybdate $Zn_{0.7}Co_{0.3}MoO_4$ (ϕ_T) shows a single wide and intense absorption band covering wavelengths ranging from 390 to 520 nm and centered at 460 nm which confirms the blue

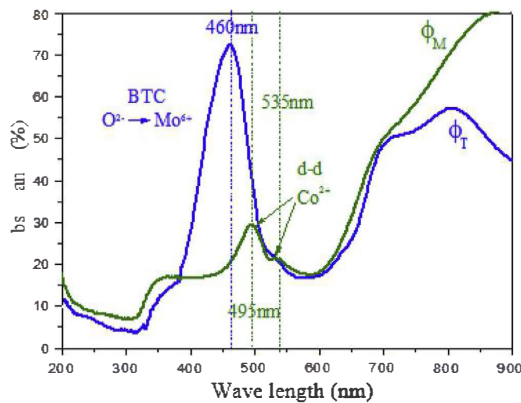


Fig. 16. UV Vis absorption spectra of $Zn_{0.7}Co_{0.3}MoO_4$ (ϕ_T) and $Zn_{0.4}Co_{0.6}MoO_4$ (ϕ_M) obtained at 700 °C.

coloration of this molybdate. This band may correspond to the charge transfer between the valence band formed by oxygen-solid atomic orbitals ($2p^6$) and the conduction band formed by empty atomic orbitals of molybdenum and/or cobalt. However, it is known that molybdenum VI is more easily reducible than cobalt II [32], so it is very probably a charge transfer $O^{2-} \rightarrow Mo^{6+}$ ($2p^6 \rightarrow 4d^0$). The energy levels of Zn empty orbitals are too high to be involved in this charge transfer [33–35]. The monoclinical molybdate $Zn_{0.4}Co_{0.6}MoO_4$ (ϕ_M) spectrum shows two absorption bands at 500 and 540 nm characteristics of the green colour. These bands of low-energy can be attributed to intra-atomic d-d transitions related to Co^{2+} ions in octahedral symmetry [33].

4. Conclusion

The molybdates $Zn_{1-x}Co_xMoO_4$ were synthesized by GNP route and solid state reactions. The X-ray analysis reveals that the compounds obtained at 700 °C present two single-phased domains regardless of the synthesis method:

- A first domain of blue colour corresponding to a level of cobalt x such as: $0 = x < 0.3$, isotype to α - $ZnMoO_4$ of triclinical symmetry.
- A second domain of green colour, for cobalt x levels such as: $0.45 = x \leq 1$ isotype to α $CoMoO_4$ of monoclinical structure.

The study by infrared and Raman spectroscopy of the compositions $x = 0.3$ and $x = 0.6$ prepared by the GNP route corroborates the formation of the solid solutions $Zn_{1-x}Co_xMoO_4$.

The UV-Visible absorption spectroscopy study confirms that the origin of blue colour ($x = 0.3$) depends on a charge transfer $O^{2-} \rightarrow Mo^{6+}$. While the green colour ($x = 0.6$) is due to intra-atomic d-d transitions related to Co^{2+} ions in octahedral symmetry.

The morphology examined by SEM and TEM analysis shows that the $Zn_{0.7}Co_{0.3}MoO_4$ powder prepared by GNP route is formed of particles of quasi-spherical morphology, with an average size of crystallites estimated between 80 - 140 nm, in acidic environment.

The colorimetric parameters measurement show the blue colour is highest for composition $x = 0.25$ in cobalt regardless of the method of synthesis adopted.

Declaration of competing interest

The authors declare that they have no known competing financial interests or personal relationships that could have appeared to influence the work reported in this paper.

Appendix A. Supplementary data

Supplementary data to this article can be found online at <https://doi.org/10.1016/j.mssp.2020.105054>.

References

- [1] V.M. Anandakumar, M.A. Khadar, Synthesis, characterization and optical properties of nanocrystalline lead molybdate, *Phys. Status Solidi A* 205 (2008) 2666–2672, <https://doi.org/10.1002/pssa.200723444>.
- [2] A.M. Huerta-Flores, I. Juárez-Ramírez, L.M. Torres-Martínez, J.E. Carrera-Crespo, T. Gómez-Bustamante, O. Sarabia-Ramos, Synthesis of $AMoO_4$ (A=Ca, Sr, Ba) photocatalysts and their potential application for hydrogen evolution and the degradation of tetracycline in water, *J. Photochem. Photobiol. Chem.* 356 (2018) 29–37, <https://doi.org/10.1016/j.jphtchem.2017.12.029>.
- [3] M. Maczka, A.G. Souza Filho, W. Paraguassu, P.T.C. Freire, J. Mendes Filho, J. Hanuza, Pressure-induced structural phase transitions and amorphization in selected molybdates and tungstates, *Prog. Mater. Sci.* 57 (2012) 1335–1381, <https://doi.org/10.1016/j.pmatsci.2012.01.001>.
- [4] B. Saravanakumar, G. Ravi, R. Yuvakkumar, V. Ganesh, R.K. Guduru, Synthesis of polyoxometalates, copper molybdate ($Cu_3Mo_2O_9$) nanopowders, for energy storage applications, *Mater. Sci. Semicond. Process.* 93 (2019) 164–172, <https://doi.org/10.1016/j.mssp.2019.01.002>.
- [5] V.D. Araújo, R.L. Tranquilin, F.V. Motta, C.A. Paskocimas, M.I.B. Bernardi, L. S. Cavalcante, J. Andres, E. Longo, M.R.D. Bomio, Effect of polyvinyl alcohol on the shape, photoluminescence and photocatalytic properties of $PbMoO_4$ microcrystals, *Mater. Sci. Semicond. Process.* 26 (2014) 425–430, <https://doi.org/10.1016/j.mssp.2014.05.027>.
- [6] K.V. Raun, L.F. Lundegaard, J. Chevallier, P. Beato, C.C. Appel, K. Nielsen, M. Thorhauge, A.D. Jensen, M. Høj, Deactivation behavior of an iron-molybdate catalyst during selective oxidation of methanol to formaldehyde, *Catal. Sci. Technol.* 8 (2018) 4626–4637, <https://doi.org/10.1039/C8CY01109E>.
- [7] Q. Li, X. Zeng, S. Yang, X. Liao, Microwave synthesis and photoluminescence properties of 3 $CaMoO_4$: Eu^{3+} nanocomposites, 2017, pp. 99–104, <https://doi.org/10.4236/ojcm.2017.72006>, 7.
- [8] L.S. Cavalcante, J.C. Szancoski, M. Siu Li, E. Longo, J.A. Varela, β - $ZnMoO_4$ microcrystals synthesized by the surfactant-assisted hydrothermal method: growth process and photoluminescence properties, *Colloid. Surface. Physicochem. Eng. Aspect.* 396 (2012) 346–351, <https://doi.org/10.1016/j.colsurfa.2011.12.021>.
- [9] L. Robertson, M. Duttine, M. Gaudon, A. Demourges, Cobalt-zinc molybdates as new blue pigments involving Co^{2+} in distorted trigonal bipyramids and octahedra, *Chem. Mater.* 23 (2011) 2419–2427, <https://doi.org/10.1021/cm200795p>.
- [10] S.F. Matar, A. Largeteau, G. Demazeau, $AMoO_4$ (A=Mg, Ni) molybdates: phase stabilities, electronic structures and chemical bonding properties from first principles, *Solid State Sci.* 12 (2010) 1779–1785, <https://doi.org/10.1016/j.solidstatesciences.2010.07.030>.
- [11] Y. Keeresta, T. Thongtem, S. Thongtem, Effect of medium solvent ratios on morphologies and optical properties of α - $ZnMoO_4$, β - $ZnMoO_4$ and $ZnMoO_4 \cdot 0.8H_2O$ crystals synthesized by microwave-hydrothermal/solvothermal method, *Superlattice. Microst.* 69 (2014) 253–264, <https://doi.org/10.1016/j.spmi.2014.02.011>.
- [12] M.-C. Liu, L.-B. Kong, C. Lu, X.-M. Li, Y.-C. Luo, L. Kang, Facile fabrication of $CoMoO_4$ nanorods as electrode material for electrochemical capacitors, *Mater. Lett.* 94 (2013) 197–200, <https://doi.org/10.1016/j.matlet.2012.12.057>.
- [13] M. Ghaed-Amini, M. Bazarganipour, M. Salavati-Niasari, K. Saberyan, Morphology and photoluminescence of $BaMoO_4$ micro- and nano-crystals synthesized by coprecipitation method, *Trans. Nonferrous Metals Soc. China* 25 (2015) 3967–3973, [https://doi.org/10.1016/S1003-6326\(15\)64045-6](https://doi.org/10.1016/S1003-6326(15)64045-6).
- [14] Z. Zhao, Z. Sui, X. Wei, J. Zuo, X. Zhang, R. Dai, Z. Zhang, Z. Ding, Structure transformation and remarkable site-distribution modulation of Eu^{3+} ions in $CaMoO_4:Eu^{3+}$ nanocrystals under high pressure, *CrystEngComm* 17 (2015) 7905–7914, <https://doi.org/10.1039/C5CE01580D>.
- [15] J. Ahmed, M. Ubiadullah, N. Alhokbany, S.M. Alshehri, Synthesis of ultrafine $NiMoO_4$ nano-rods for excellent electro-catalytic performance in hydrogen evolution reactions, *Mater. Lett.* 257 (2019), 126696, <https://doi.org/10.1016/j.matlet.2019.126696>.
- [16] V. Umapathy, P. Neeraja, A. Manikandan, P. Ramu, Synthesis of $NiMoO_4$ nanoparticles by sol-gel method and their structural, morphological, optical, magnetic and photocatalytic properties, *Trans. Nonferrous Metals Soc. China* 27 (2017) 1785–1793, [https://doi.org/10.1016/S1003-6326\(17\)60201-2](https://doi.org/10.1016/S1003-6326(17)60201-2).
- [17] A. Kumar Mishra, Sol-gel Based Nanoceramic Materials, Springer Berlin Heidelberg, New York, NY, 2016, <https://doi.org/10.1007/978-3-319-49512-5>.
- [18] K. Seevakan, A. Manikandan, P. Devendran, A. Baykal, T. Alagesan, Electrochemical and magneto-optical properties of cobalt molybdate nano-catalyst as high-performance supercapacitor, *Ceram. Int.* 44 (2018) 17735–17742, <https://doi.org/10.1016/j.ceramint.2018.06.240>.
- [19] V. Srirapu, A. Kumar, N. Kumari, P. Srivastava, R.N. Singh, A comparative study of electrocatalytic performance of metal molybdates for the water oxidation, *Int. J. Hydrogen Energy* 43 (2018) 16543–16555, <https://doi.org/10.1016/j.ijhydene.2018.07.060>.
- [20] K. Nakamoto, *Infrared and Raman Spectra of Inorganic and Coordination Compounds: Part A: Theory and Applications in Inorganic Chemistry*, sixth ed., 2009.
- [21] B.J. Reddy, P. Vickraman, A.S. Justin, A facile synthesis of novel α - $ZnMoO_4$ microspheres as electrode material for supercapacitor applications, *Bull. Mater. Sci.* 42 (2019) 52, <https://doi.org/10.1007/s12034-019-1749-9>.
- [22] H. Lakhliji, M. Benchikhi, R. El Ouatib, L. Er-Rakho, S. Guillemet, B. Durand, Synthesis and physicochemical characterization of pigments based on molybdenum α - $ZnO-MoO_3:Co^{2+}$, *J. Mater. Environ. Sci.-JMES* 6 (2015) 3465–3469.
- [23] P. Yadav, E. Sinha, Structural, photophysical and microwave dielectric properties of α - $ZnMoO_4$ phosphor, *J. Alloys Compd.* 795 (2019) 446–452, <https://doi.org/10.1016/j.jallcom.2019.05.019>.
- [24] J. Fu, J.-L. Meng, M.-J. Wei, H.-Y. Zang, H.-Q. Tan, Y.-H. Wang, H. Miras, Y.-G. Li, Cross-linked $CoMoO_4/rGO$ nanosheets as oxygen reduction catalyst, *Catalysts* 7 (2017) 375, <https://doi.org/10.3390/catal7120375>.
- [25] P.J. Mafa, B. Ntsendwana, B.B. Mamba, A.T. Kuvarega, Visible light driven $ZnMoO_4/BiFeWO_6/rGO$ Z-scheme photocatalyst for the degradation of anthraquinonic dye, *J. Phys. Chem. C* 123 (2019) 20605–20616, <https://doi.org/10.1021/acs.jpcc.9b05008>.
- [26] B. Bakiz, F. Guinneton, J.R. Gavarrí, Structural and Temperature-dependent vibrational analyses of the non-centrosymmetric $ZnMoO_4$ molybdate, *J. Mater. Environ. Sci.* 7 (2016) 3076–3083.
- [27] N. Padmanathan, H. Shao, S. Selladurai, C. Glynn, C. O'Dwyer, K.M. Razeeb, Pseudocapacitance of α - $CoMoO_4$ nanoflakes in non-aqueous electrolyte and its bifunctional electro catalytic activity for methanol oxidation, *Int. J. Hydrogen Energy* 40 (2015) 16297–16305, <https://doi.org/10.1016/j.ijhydene.2015.09.127>.
- [28] T. Meng, H. Jia, H. Ye, T. Zeng, X. Yang, H. Wang, Y. Zhang, Facile preparation of $CoMoO_4$ nanorods at macroporous carbon hybrid electrocatalyst for non-enzymatic glucose detection, *J. Colloid Interface Sci.* 560 (2019) 1–10, <https://doi.org/10.1016/j.jcis.2019.10.054>.

- [29] Y. Chen, Y. Wang, X. Shen, R. Cai, H. Yang, K. Xu, A. Yuan, Z. Ji, Cyanide-metal framework derived $\text{CoMoO}_4/\text{Co}_2\text{O}_4$ hollow porous octahedrons as advanced anodes for high performance lithium ion batteries, *J. Mater. Chem. A*. 6 (2018) 1048–1056, <https://doi.org/10.1039/C7TA08868J>.
- [30] F. Nti, D.A. Anang, J.I. Han, Facilely synthesized $\text{NiMoO}_4/\text{CoMoO}_4$ nanorods as electrode material for high performance supercapacitor, *J. Alloys Compd.* 742 (2018) 342–350, <https://doi.org/10.1016/j.jallcom.2018.01.289>.
- [31] L. Fang, F. Wang, T. Zhai, Y. Qiu, M. Lan, K. Huang, Q. Jing, Hierarchical CoMoO_4 nanoneedle electrodes for advanced supercapacitors and electrocatalytic oxygen evolution, *Electrochim. Acta* 259 (2018) 552–558, <https://doi.org/10.1016/j.electacta.2017.11.012>.
- [32] D.A. Kuznetsov, Z. Chen, P.V. Kumar, A. Tsoukalou, A. Kierzkowska, P.M. Abdala, O.V. Safonova, A. Fedorov, C.R. Müller, Single site cobalt substitution in 2D molybdenum carbide (MXene) enhances catalytic activity in the hydrogen evolution reaction, *J. Am. Chem. Soc.* 141 (2019) 17809–17816, <https://doi.org/10.1021/jacs.9b08897>.
- [33] M. Pirhashemi, A. Habibi-Yangjeh, Facile fabrication of novel $\text{ZnO}/\text{CoMoO}_4$ nanocomposites: highly efficient visible-light-responsive photocatalysts in degradations of different contaminants, *J. Photochem. Photobiol. Chem.* 363 (2018) 31–43, <https://doi.org/10.1016/j.jphotochem.2018.05.027>.
- [34] R.K.S. Costa, S.C. Teles, P.C. de Sousa Filho, A. Dias, K.P.F. Siqueira, Influence of europium doping on the structural phase-transition temperature of β - and α - CoMoO_4 polymorphs, *Mater. Res. Bull.* 118 (2019), 110517, <https://doi.org/10.1016/j.materresbull.2019.110517>.
- [35] V. Jeseentharam, A. Dayalan, K.S. Nagaraja, Co-precipitation synthesis, humidity sensing and photoluminescence properties of nanocrystalline Co^{2+} substituted zinc (II)molybdate ($\text{Zn}_{1-x}\text{Co}_x\text{MoO}_4$; $x = 0, 0.3, 0.5, 0.7, 1$), *Solid State Sci.* 67 (2017) 46–58, <https://doi.org/10.1016/j.solidstatesciences.2017.02.008>.